Interferometric Performance of a Cartwheel Constellation for TerraSAR-L

Manfred Zink[(1)] , Gerhard Krieger [(2)] , Thierry Amiot [(3)]

[(1)] ESA/ESTEC, E-Mail: Manfred.Zink@esa.int
[(2)] Microwaves and Radar Institute, German Aerospace Center (DLR), E-Mail: Gerhard.Krieger@dlr.de
[(3)] Centre National d'Etudes Spatiales (CNES), E-Mail: Thierry.Amiot@cnes.fr

ABSTRACT

This paper provides a prediction of the achievable interferometric performance for a TerraSAR-L cartwheel constellation. Assuming receiving antennas of only 3m diameter, ambiguity and noise floor levels are analysed in detail. Expected DEM accuracies for different effective baselines at different swath positions including effects of local slope and volume decorrelation over vegetation are presented.

1. INTRODUCTION

Synthetic aperture radar interferometry is a powerful and well established remote sensing technique to extract important bio- and geophysical parameters about the Earth's surface (Bamler, 1998, Rosen, 2000). The great potentials of SAR interferometry have been demonstrated in numerous examples. However, the currently available data from spaceborne SAR sensors suffer either from temporal and atmospheric disturbances (repeat pass interferometry) or from a limited interferometric baseline (SRTM). To overcome these limitations, several suggestions have been made to acquire interferometric data in a single pass by using two or more independent radar satellites operating in a fully or semi-active SAR mode (Zebker, 1994, Massonnet, 1998, Das, 1998, Martin, 2001). The idea of using passive micro-satellites flying in formation with a conventional SAR, as introduced by D. Massonnet in 1998, is especially attractive, since it will enable a cost efficient implementation of a highly capable interferometric single pass SAR system in space. Detailed performance analyses demonstrated the great potentials of such a concept (Krieger, 2003, Amiot, 2002).

The European Space Agency (ESA) has initiated and supported an investigation to analyse the option of adding such an interferometric constellation of passive receiver satellites to the TerraSAR-L mission. Primary objective is the generation of a global DEM of HRTI level-3 quality. Ocean current monitoring is another important application facilitated by such a single-pass InSAR configuration. The constellation will be regarded as an integral element of TerraSAR-L, i.e. special modes exploiting the full capabilities of the main spacecraft will allow for an improved performance. Furthermore inter satellite links can be used to synchronise the data recording and provide TT&C communication and science data downlink via TerraSAR-L and hence simplify the micro satellite architecture. In the study, several orbital configurations have been investigated in detail and compared with each other. The following sections summarise the results of a comprehensive interferometric performance analysis for such a distributed satellite constellation. These results have been obtained in a close cooperation between CNES, DLR and ESA.

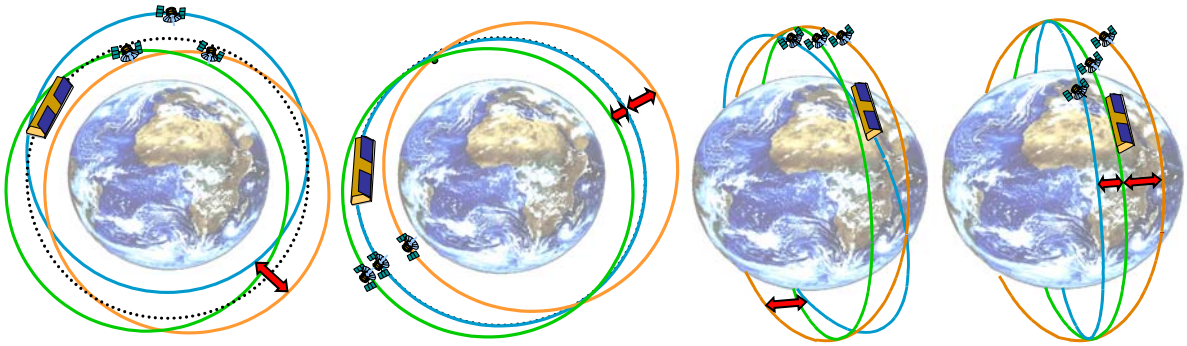

Figure 1: Examples of interferometric satellite constellations investigated by CNES and DLR during the TerraSAR-L cartwheel constellation study. From left to right: Interferometric Cartwheel (CNES), Two-Scale Cartwheel (CNES), Cross-Track Pendulum (DLR), and Trinodal Pendulum (DLR). The Trinodal Pendulum and the Two-Scale Cartwheel allow for the simultaneous acquisition of multiple interferometric baselines at a constant baseline ratio.

Proc. of FRINGE 2003 Workshop, Frascati, Italy,
1 – 5 December 2003 (ESA SP-550, June 2004) 125_krieger

2. AMBIGUITY ANALYSIS

The antennas of the passive receivers in the TerraSAR-L cartwheel constellation will be substantially smaller than the 11 m by 2,86 m aperture of TerraSAR-L. Small antennas are a prerequisite for an accommodation of all satellites in a common launcher. The allowed antenna size and its shape is further limited by the maximum momentum that can be handled by a microsatellite. For the scope of this investigation, it was decided to assume circular receiver antennas with a radius of 1,5 m. The small aperture of the receiver antennas may cause a rise of the ambiguity level. Hence, a detailed ambiguity analysis has been conducted.

Figure 2 shows the range ambiguity to signal ratio as a function of ground range position relative to the swath centre and the pulse repetition frequency (PRF) for incident angles of 30° (upper left), 35° (upper right), 40° (lower left), and 45° (lower right). The red arrows indicate the maximum PRF for a range ambiguity to signal ratio of –20 dB and a swath width of 40 km and 70 km, respectively. From Figure 2 it becomes clear that range ambiguities will limit the maximum PRF especially at large incident angles. On the other hand, the short antenna length of the passive receiver satellites will cause an azimuth antenna pattern with a broad mainlobe. Hence, the level of the azimuth sidelobes in the joint antenna pattern will be substantially increased, thereby increasing also the required PRF. To alleviate this effect, three different tapering functions for TerraSAR-L have been investigated during this study: (1) Taylor, (2) Hamming, and (3) Dolph-Tschebyscheff tapering. Figure 3 shows the azimuth ambiguity to signal ratio as a function of the PRF for constant tapering (red), Taylor tapering (yellow), Hamming tapering (green), and Dolph-Tschebyscheff tapering (blue) at a processed bandwidth of 1,0 kHz (dashed) and 1,2 kHz (solid). It is clear, that azimuth tapering of the TerraSAR-L antenna pattern is an appropriate means to reduce azimuth ambiguities. For example, Hamming weighting will reduce azimuth ambiguities by ca. –5 dB for the interesting PRF range between 2 kHz and 2,5 kHz. A final optimisation of the tapering is beyond the scope of this investigation, but the exemplary results in this study show the potentials of such an optimisation for a significant reduction of ambiguities.

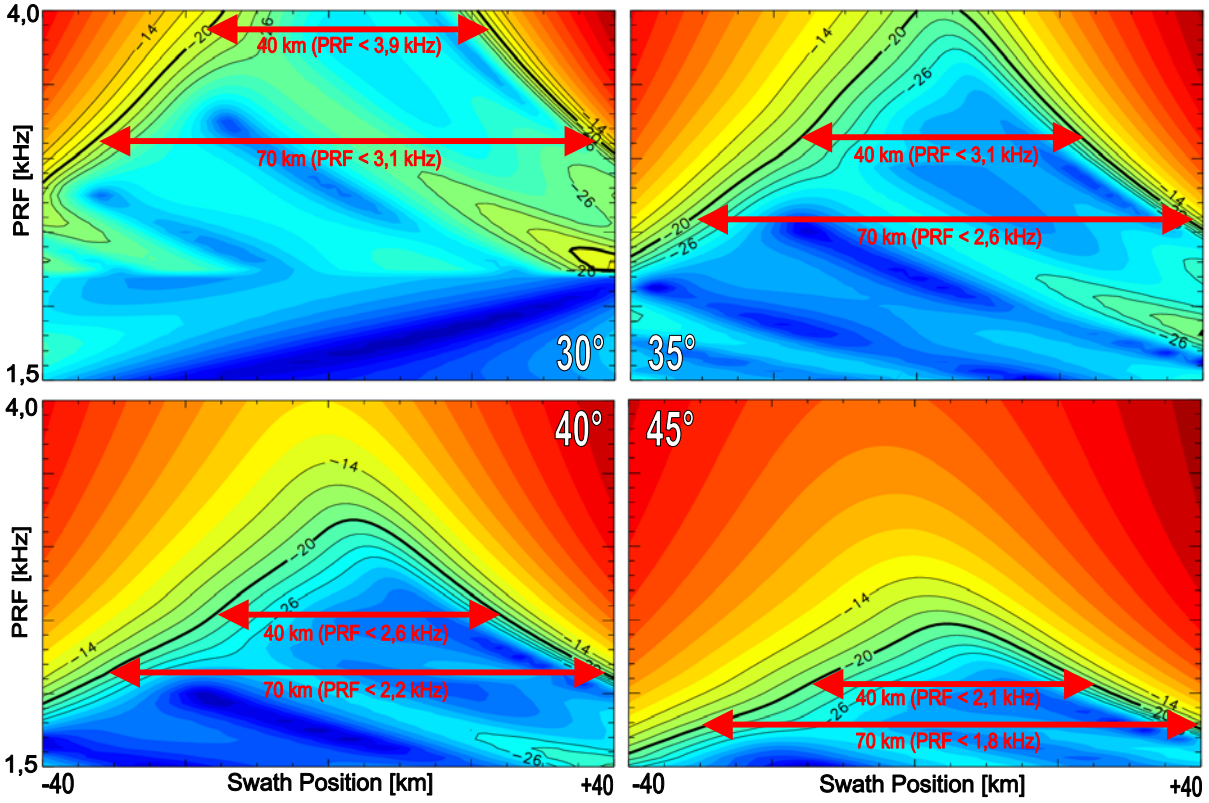

Figure 2: Range ambiguity to signal ratio (RASR) as a function of swath position and PRF for incident angles of 30° (upper left), 35° (upper right), 40° (lower left), and 45° (lower right).

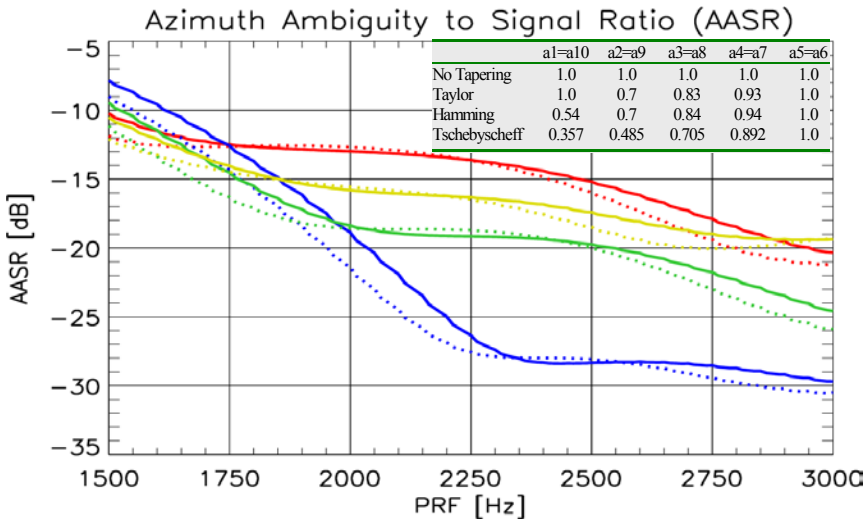

Figure 3: Azimuth ambiguities as a function of the PRF for constant (red), Taylor (yellow), Hamming (green), and Dolph-Tschebyscheff (blue) tapering. The processed Doppler bandwidths are 1000 Hz (dotted) and 1200 Hz (solid), respectively. The tapering coefficients for the different weighting functions are shown in the inset on the upper right.

3. DERIVATION OF HEIGHT ERRORS

3.1 System Parameters and Beam Selection

In the following, we will outline the derivation of the relative height accuracy. The system parameters of the investigated configuration are shown in the upper part of Table 1. For illustration purposes, we assume a data acquisition of a 168 km swath using three sub-swaths. The value of 168 km corresponds to the separation of the satellite ground tracks at the equator after one full repeat cycle of 16 days. The lower part of Table 1 summarises the main parameters of the selected subswaths. Two additional subswaths have been introduced to show the performance for a data acquisition at lower and higher incident angles. Such additional beams may for example be used to resolve problems at low incident angles (e.g. due to foreshortening) or to improve the performance at higher incident angles that only offer a reduced SNR. The subswath selection results from a first, rough iteration which had the goal to optimise the DEM performance across a swath of 168 km with a minimum number of subswaths. In this example, only three passes would be required at the equator, thereby minimising the total acquisition time for a global DEM. A first analysis shows that a global DEM can be obtained within 1 year mission time.

System Parameters					
Frequency	1.2575 GHz		Duty Cycle	7 %	
Chirp Bandwidth	80 MHz		Post-spacing	12 m x 12 m	
Tx-Power	6400 W		Sigma Nought	Shrubs, L-Band, HH	
Losses (Tx)	1.3 dB		Tx-antenna	11 m x 2.86 m	
Losses (Atm)	1.0 dB		Rx-antenna	3 m ring focus (CNES)	
Losses (Rx)	1.5 dB		Co-Registration Accuracy	1/10 pixel	
Noise Figure	2.5 dB		Quantization	BAQ with 4 bit/sample	
Swath Selection					
Swath Width	75 km	70 km	60 km	50 km	50 km
Antenna Look Angle	25.2	29.2	33.7	36.6	38.8
Incident Angles [deg]	24.6 – 30.6	30.3 – 35.5	35.2 – 39.3	39.0 – 42.2	42.0 – 44.9
PRF [Hz]	2950	2190	2490	2200	1950
Ground Range [km]	259 – 334	330 – 400	396 – 456	452 – 502	498 – 548
Antenna Tapering	None	Taylor	None	Taylor	Taylor
Processed Bandwidth [Hz]	1200	1200	1000	1200	1200

Table 1: Summary of System, Processing, and Beam Parameters

3.2 Derivation of Interferometric Phase Errors

Table 2 summarises some intermediate results of the performance analysis. The Noise Equivalent Sigma Zero (NESZ) for the investigated subswaths is shown in Table 2 on the upper left (red and blue lines). For comparison, the figure shows also the L-Band backscattering coefficients for shrubs from (Ulaby & Dobson 1989) for HH polarisation and an occurence level of 50% (green dotted line). The results from the ambiguity analysis are shown in Table 2 on the upper right. Range ambiguities are in solid and azimuth ambiguities in dotted style. The range and azimuth ambiguity ratios reach levels of up to ~ -16dB. Such and even higher ambiguity levels can be tolerated, if the contribution of ambiguities to the final interferogram can be treated as additive white noise, since the thermal noise due to the limited NESZ exceeds the ambiguity level and will clearly dominate the phase noise in the final interferogram. Note in this context, that it would be no problem to further reduce the ambiguities by a more stringent azimuth tapering and/or by an optimised selection of appropriate PRFs. The results from the coherence analysis are shown in Table 2 on the lower left. The solid lines are for the total coherence while the dotted and dashed lines illustrate the contributions from the thermal noise and the ambiguities treated as white noise, respectively. The interferometric phase errors after multi-looking are shown in Table 2 on the lower right, assuming an independent post-spacing of 12 m x 12 m as required by the emerging NIMA HRTI level-3 standard.

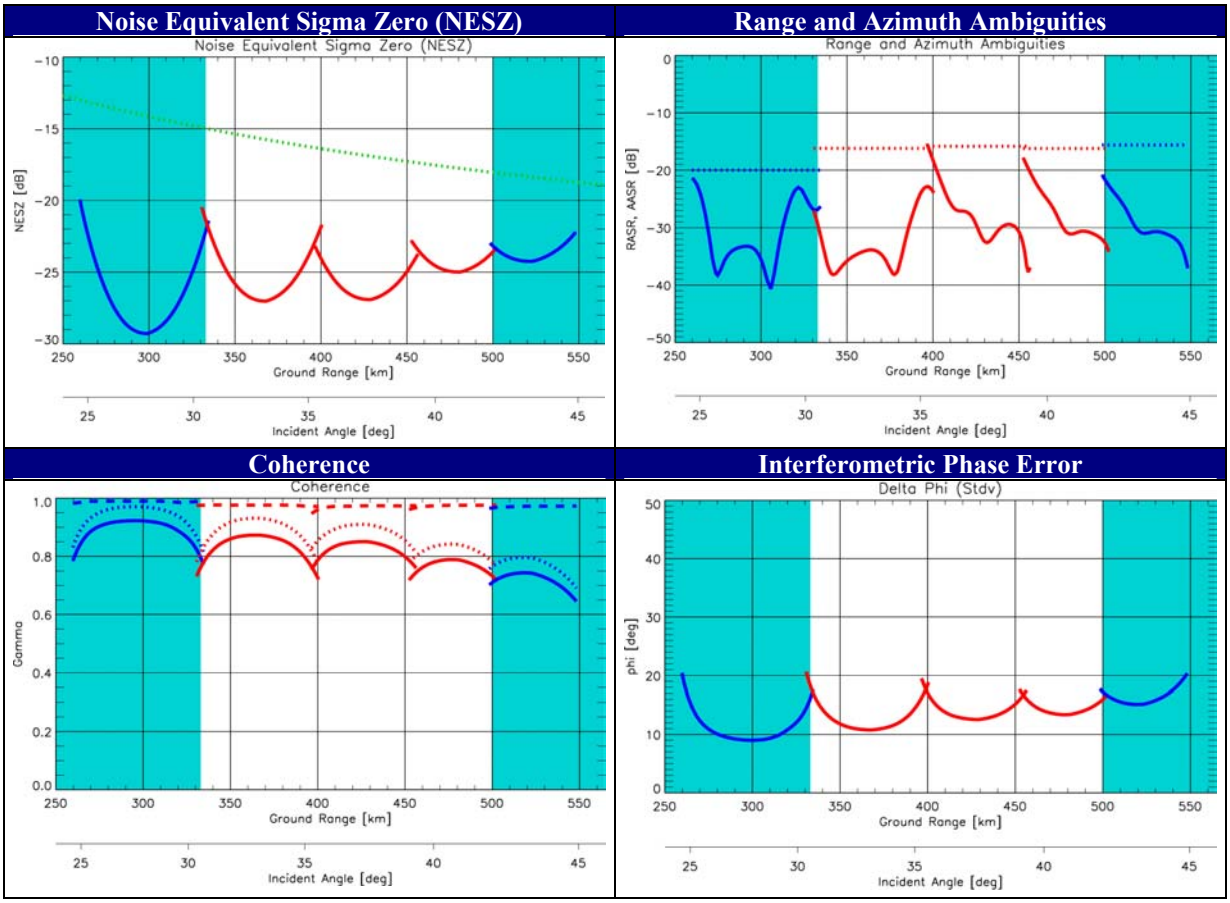

Table 2: Summary of major intermediate steps in the performance analysis (cf. text).

3.3 Height Accuracy and Height of Ambiguity

Figure 4 shows the predicted height accuracy for a height of ambiguity of 100 m (dashed) and 10 m (dotted). It is obvious, that the height accuracy increases with a decreasing height of ambiguity. On the other hand, a small height of ambiguity is likely to cause phase wrapping problems, especially in mountainous areas. The baseline ratio of the example in Figure 4 has been chosen such that the height errors from the DEM acquisition with the small baseline stay below the height of ambiguity for the large baseline. It would hence be possible to use the interferometric data from the small baseline to assist phase unwrapping in the highly sensitive large baseline interferogram. The opportunity to have an excellent height accuracy in combination with a large height of ambiguity was also the major reason for suggesting the Trinodal Pendulum and the Two-Scale Cartwheel, which will both allow for the simultaneous acquisition of large and small baselines in a single pass (cf. Figure 1). The exact value of the optimum baseline ratio will depend on several factors like incident angle, scattering

coefficients, terrain type, etc., and clearly deserves further investigation. A first, rather conservative suggestion is to use a baseline ratio of 5 to 1 which will allow for a final height accuracy below 1 m with an initial height of ambiguity of 100 m.

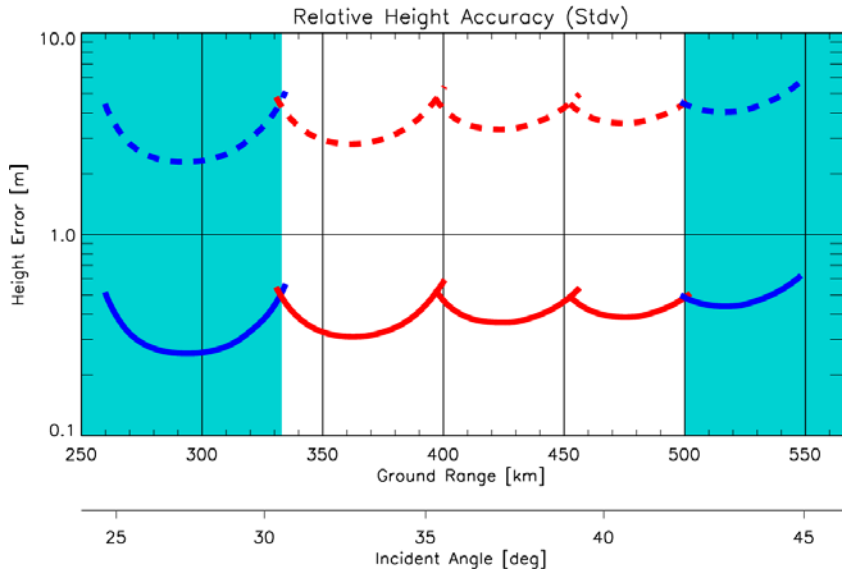

Figure 4: Predicted height accuracy for a height of ambiguity of 100 m (dashed) and 10 m (solid)

3.4 Local Slopes

The HRTI level-3 specification will require full performance for mountainous terrain with slopes up to 20%. Figure 5 shows the results of a performance estimation for forward (dashed) and backward (dotted) slopes of 20% assuming an effective baseline of 6 km. In general, the height accuracy is increased for forward slopes facing towards the radar and reduced for backward slopes facing away from the radar. This is mainly due to a change of the scattering coefficient. Only at small incident angles, it might be possible that the loss in spatial resolution due to range filtering dominates the height error. This effect will be small for a high bandwidth system, but it may become more critical with reduced chirp bandwidth. As can be seen, the height errors remain always below 1,0 m across the whole 168 km swath in case of flat areas. Backward slopes will slightly increase the height errors to 1,3 m while forward slopes will cause a reduction of the height errors to 0,7 m. The effect of slopes may further be mitigated by combining data from ascending and descending orbits and/or from acquisitions with different incident angles.

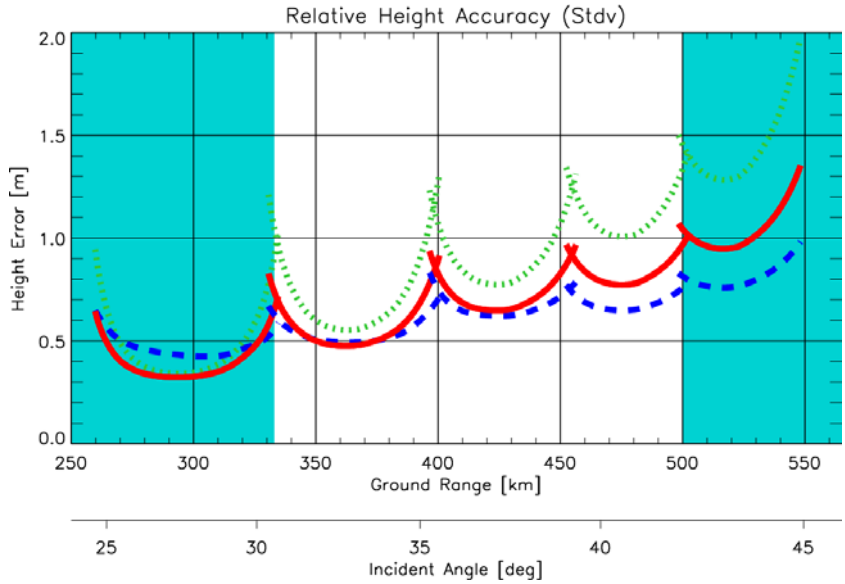

Figure 5: Predicted height accuracy for an effective baseline of 6 km (solid) and impact of forward (dashed) and backward (dotted) slopes. The slope is 20%.

3.5 Volume Decorrelation

Volume scattering in vegetated areas will reduce the coherence of the interferometric signal and hence the achievable height accuracy. The increased 'phase noise' in case of large baselines and high volumes may also cause significant problems with phase unwrapping. Figure 6 shows an estimate of the impact of volume decorrelation on the relative height error for a typical extinction coefficient of 0,2 dB/m and volume heights of 5 m (yellow), 10 m (orange) and 20 m (green). The left plot is for an effective baseline of 1,2 km and the right plot is for an effective baseline of 6 km. It is clear, that the additional 'noise' due to volume scattering depends strongly on the length of the interferometric baseline. While the additional noise is quite small for the 1,2 km baseline, it may almost completely destroy the signal in case of the 6 km baseline as soon as the volume height exceeds a value of 10 m.

The deteriorating effect of volume decorrelation can be substantially reduced by selecting smaller baselines as provided in the Trinodal Pendulum or the Two-Scale Cartwheel (cf. Figure 1). Hence, the simultaneous interferometric data acquisition with large and small baselines will help to acquire valuable data over both bare and vegetated areas. It is expected, that further information can be gained from a joint evaluation of the interferometric data acquired with different baselines, but this topic clearly deserves further investigation. In homogeneous areas, volume decorrelation can also be reduced by increasing the size of the independent post-spacing.

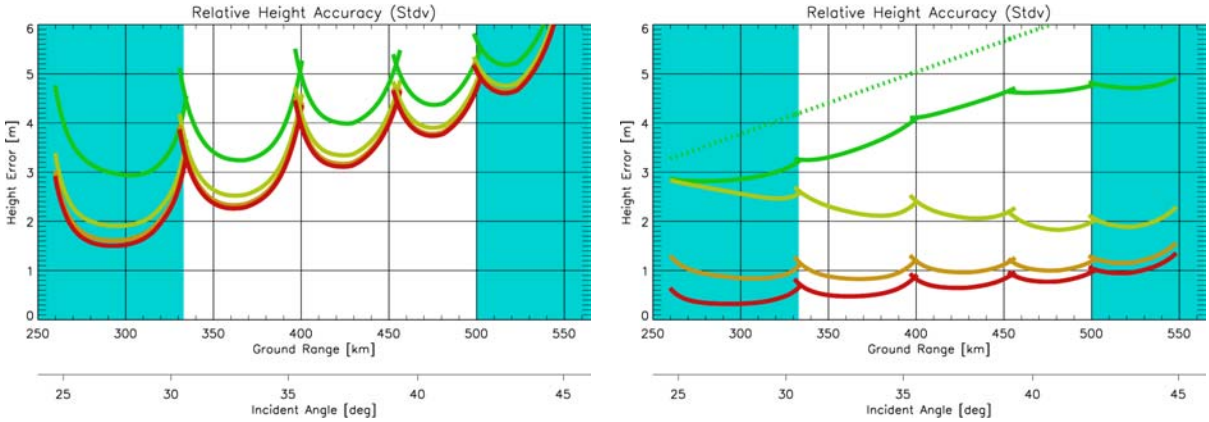

Figure 6: Impact of volume scattering on the achievable height accuracy for an effective baseline of 1,2 km (left) and an effective baseline of 6 km (right). The extinction coefficient is 0,2 dB/m and the volume heights are 0 m (red/blue), 5 m (orange), 10 m (yellow), and 20 m (green).

4. DISCUSSION

The results from the performance estimation show, that a relative height accuracy below the 1m level can be achieved by enhancing TerrSAR-L with an appropriately designed interferometric microsatellite constellation. The required effective baselines are in the order of 5 km. Such baselines will lead to a height of ambiguity which may become as small as 15 m. Phase unwrapping would hence require very precise a priori information. This requirement can be avoided by a second interferometric data acquisition with a shorter baseline. Elegant solution for the acquisition of such a second baseline are the Trinodal Pendulum or the Two-Scale Cartwheel, which offer the opportunity to acquire short and long baselines simultaneously during one single pass (cf. Figure 1). By this, they make effective use of the available resources from the transmitter (e.g. signal power, illumination time, etc.). Furthermore, possible errors due to temporal changes between subsequent scene acquisitions are avoided. Such changes may for example be caused by different target conditions, different system temperatures, or uncompensated attitude/orbit errors. The co-registration of the interferometric acquisitions with different baselines will also be simplified. The baseline ratio should be chosen such that the height of ambiguity of the coarse DEM is as high as possible, but the height accuracy of the coarse DEM must still be better than the height of ambiguity of the high resolution DEM obtained with the large baseline. From a first assessment of the estimated phase errors, it is suggested to use baseline ratios in the order of 5 to 1 (the third baseline will then have a ratio of 4 to 1). In this case, the height of ambiguity will be always greater than 75 m for a height accuracy below 1m. Given some a priori information from other DEMs, it is expected that this will solve most phase unwrapping problems, but it is still possible to acquire data from problematic areas with smaller baselines during another mission phase. The conservative assumption of a baseline ratio of 5 to 1 could also be increased, especially if a larger number of looks with a larger independent post spacing will be used for the coarse DEM. In this case, the increased ground resolution may still provide sufficient information for phase unwrapping, except for isolated peaks. The height accuracy can further be improved by a combination of

interferograms from ascending and descending orbits and/or acquisitions with different incident angles and different baselines.

Our analyses have shown, that the TerraSAR-L cartwheel constellation will be an excellent means to acquire a global DEM with unprecedented height accuracy in accordance with the HRTI level-3 specification. This emerging standard for digital elevation models requires a relative height accuracy of 2 m for point to point errors at 90% occurence levels and an independent post spacing of 12m. The required mission time will be in the order of 1 year assuming an average data collection of 3 minutes per orbit. In a later mission phase, the performance may even be improved beyond the HRTI level-3 specification by increasing the length of the interferometric baselines.

5. ACKNOWLEDGEMENT

We would like to thank R. Torres, B. Duesmann, and G. Levrini from ESA for initiation and support of this work. The numerous and fruitful discussions with F. Douchin, M. Werner, J. Fourcade, H. Fiedler, J.C. Souyris, F. Jochim, C. Jouve, H. Runge, A. Moreira, F. Rocca, R. Romeiser, K. Papathanassiou, and I. Hajnsek during the joint ESA-DLR-CNES meetings are greatly appreciated. Financial support for this work came from ESA.

6. REFERENCE

Amiot, T., Douchin, F., Thouvenot, E., Souyris, J.C., Cugny, B., **2002**, "The Interferometric Cartwheel: A Multi-Purpose Formation of Passive Radar Microsatellites", Proc. of the IGARSS'02, pp. 435-437

Bamler, R. & Hartl, P., **1998**, "Synthetic Aperture Radar Interferometry", Inverse Problems, Vol. 14, pp. R1-R54

Das, A., Cobb, R., *TechSat 21 - Space Missions Using Collaborating Constellations of Satellites*, 1998.

Krieger, G., H. Fiedler, J. Mittermayer, K. Papathanassiou, and A. Moreira **2003**, "Analysis of multistatic configurations for spaceborne SAR interferometry", IEE Proc. Radar Sonar Navigation, Vol. 150, No. 3, pp. 87- 96.

Massonnet, D., **1998**, "Roue interferometrique", French Patent no 236910D17306RS

Massonnet, D., **2001**, "Capabilities and Limitations of the Interferometric Cartwheel", IEEE Trans. Geosci. Remote Sensing, Vol. 39, No. 3, pp. 506-520

Martin M., Klupar P., Kilberg S., Winter J., TechSat 21 and Revolutionizing Space Missions Using Microsatellites, American Institute of Aeronautics and Astronautics, 2001.

Rodriguez, E. & Martin, J.M., **1992**, "Theory and Design of Interferometric Synthetic Aperture Radars", IEE Proceedings-F, Vol. 139, No. 2, pp. 147-159

Rosen, P.A., Hensley, S., Joughin, I.R., Li, F.K., Madsen, S.N., Rodriguez, E., Goldstine, R., **2000**, "Synthetic Aperture Radar Interferometry", Proc. IEEE, Vol. 88, No. 3, pp. 333-382

Ulaby, F.T. & Dobson, M.C., **1989**, "Handbook of Radar Scattering Statistics for Terrain", Artech House, Norwood, MA

Zebker, H.A., Farr, T.G., Salazar, R.P., Dixon, T.H., **1994**, "Mapping the World's Topography Using Radar Interferometry: The TOPSAT Mission", Proc. IEEE, Vol. 82, No. 12, pp. 1774-1786

Zink, M., *Definition of the TerraSAR-L Cartwheel Constellation*, ESA TS-SW-ESA-SY-0002, ESTEC, Noordwijk, 2003.